

Fast tunnel rates in Si/SiGe one-electron single and double quantum dots

Madhu Thalakulam,^{a)} C. B. Simmons, B. M. Rosemeyer, D. E. Savage, M. G. Lagally, Mark Friesen, S. N. Coppersmith, and M. A. Eriksson
University of Wisconsin-Madison, Madison, Wisconsin 53706, USA

(Received 3 March 2010; accepted 15 April 2010; published online 4 May 2010)

We report the fabrication and measurement of one-electron single and double quantum dots with fast tunnel rates in a Si/SiGe heterostructure. Achieving fast tunnel rates in few-electron dots can be challenging, in part due to the large electron effective mass in Si. Using charge sensing, we identify signatures of tunnel rates in and out of the dot that are fast or slow compared to the measurement rate. Such signatures provide a means to calibrate the absolute electron number and verify single electron occupation. Pulsed gate voltage measurements are used to validate the approach. © 2010 American Institute of Physics. [doi:10.1063/1.3425892]

The spins of electrons isolated in quantum dots are promising candidates for solid-state qubits.¹ Spin readout and manipulation have been demonstrated in GaAs quantum dots, using both one and two-electron spin states as logical qubits.^{2–4} To enable successful error correction, it is advantageous to have spin dephasing times and lifetimes as long as possible. Because isotopes of Si with zero nuclear spin exist, resulting in particularly slow electron spin dephasing and long lifetimes,^{5–7} a number of proposals have been made for spin qubits based on confined electrons in Si quantum dots and donors.^{8–12} There has been significant progress in the development of quantum dots in Si (Refs. 13–25) but achieving single-charge occupation in Si dots is challenging. One issue is the relatively large electron effective mass m^* in Si, which leads to smaller tunnel rates than would arise for the same size and shape barrier in materials with lighter m^* . While occupation of Si single quantum dots by individual charges has been demonstrated for both electrons^{26,27} and holes,²⁸ a double quantum dot with a single electron in each dot, the foundation for coupled qubits, or the two-electron singlet-triplet qubit,²⁹ has not been achieved until now.

This paper reports the demonstration of Si/SiGe single and double quantum dots occupied by zero, one, and two electrons, and it describes signatures of fast tunnel rates in the one-electron limit for these dots. We show that tunnel rates in Si/SiGe quantum dots change noticeably over moderate gate voltage ranges that correspond to removing several electrons from the quantum dot. This change is rapid enough to require retuning of the tunnel barriers in and out of the dot when approaching the one-electron state. By careful tuning of the gate voltages, we can measure reliably the expulsion of the last electron from the quantum dot, providing an absolute reference for charge counting. By using pulsed gate voltages in combination with charge sensing, we demonstrate electron tunneling at rates as high as 2 MHz in a one-electron single quantum dot and 50 kHz in a one-electron double quantum dot.

The quantum dot used in this work is formed in a Si/SiGe heterostructure containing a two-dimensional electron gas approximately 79 nm below the crystal surface, with a carrier density of $5.15 \times 10^{11} \text{ cm}^{-2}$ and mobility of $120\,000 \text{ cm}^2/\text{V s}$, after illumination with red light for 10 s

while at a temperature of 4.2 K at the beginning of the experiment. The heterostructure consists of an undoped relaxed buffer of Si/Si_{0.71}Ge_{0.29}, a strained-Si quantum well 18 nm thick, 22 nm undoped Si/Si_{0.71}Ge_{0.29}, 2.6 nm phosphorus-doped Si/Si_{0.71}Ge_{0.29}, 45 nm undoped Si/Si_{0.71}Ge_{0.29}, and a 9 nm Si cap layer. Figure 1(a) shows a scanning electron micrograph of a device with the same gate structure as that reported here. The top-gates are formed by electron-beam evaporation of Pd onto the HF-etched surface of the heterostructure, following a gate design similar to Ref. 30. The gates sit on a square mesa of width 35 μm defined by reactive ion etching. The squares at the four corners represent the directions toward available Ohmic contacts. All measurements were performed in a dilution refrigerator with a mixing chamber temperature below 20 mK.

The quantum dot is formed by the application of negative voltages to gates L , M , R , and T . The dot is tuned to the few-electron regime by making the voltages on the gates more negative. Two charge sensing point contacts are formed by the application of negative voltage to the left (Q_L) and right (Q_R) quantum point contact (QPC) gates. Figure 1(b) is a plot of the transconductance $g = \partial I_{\text{QPC}} / \partial V_M$ as a function of V_M , where I_{QPC} is the current through the left point contact. The regularly spaced peaks in g represent changes in the charge occupation of the dot of one electron. Figure 1(c) shows g as a function of V_M and V_L ; the peaks in g lie along straight lines, indicating that the device is a single quantum dot in this gate voltage regime.

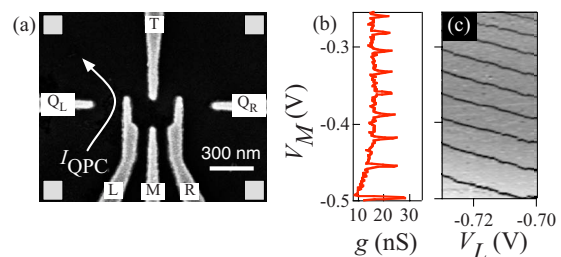


FIG. 1. (Color online) (a) Scanning electron micrograph of the top-gates that define the active region of the device. (b) The transconductance g of the charge-sensing QPC as a function of V_M . Peaks in g represent electron tunneling events. (c) Plot of g vs the gate voltages V_M and V_L . The dark lines indicate electron tunneling events and are parallel, showing that the device is a single quantum dot in this gate voltage regime.

^{a)}Electronic mail: thalakulam@wisc.edu.

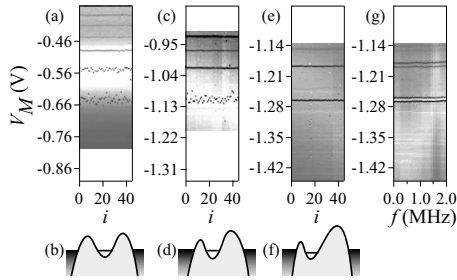


FIG. 2. Demonstration of fast and slow electron tunneling between the leads and the quantum dot (horizontal black lines). Panels (a), (c), and (e) show the QPC transconductance g as a function of V_M for repeated sweeps, labeled with the index i . The gate voltage conditions are as follows: (a) $V_L = -0.725$ V, $V_R = -0.83$ V, (c) $V_L = -0.65$ V, $V_R = -0.94$ V, and (e) $V_L = -0.54$ V, $V_R = -0.965$ V. The plots are arranged so that the corresponding charge transitions are aligned. Panels (b), (d), and (f) show schematic diagrams of the potential landscape for the plot above each diagram. (g) Time-averaged charge sensing in the presence of a pulsed gate voltage for the same conditions as panel (e): g as a function of V_M and pulse frequency f .

A key question is how to assess whether the last observable line in a plot such as that shown in Fig. 1(c) represents the removal of the last electron in the quantum dot. One typically expects the changes in gate voltage ΔV_G to become nonuniform as the last electron is approached.²⁶ A concern that is sometimes raised is whether the tunnel rate into the dot has become sufficiently slow that an additional transition is simply missed. This concern is perhaps especially well taken in Si, because the effective mass of electrons in silicon ($m^* = 0.19m_e$) is higher than that in GaAs ($m^* = 0.067m_e$), the most widely studied host for semiconductor quantum dots. Because of its relatively large m^* , tunnel rates in Si will vary much more strongly as the tunnel barrier is changed than in GaAs. As a result, care must be taken, in device design and in experimental measurements, to ensure that the tunnel barriers do not turn opaque as gate voltages are made more negative and the few electron regime is reached. We show that such changes in tunnel rates yield clear signatures in the data, enabling the device used here to be reliably tuned to a regime with fast tunnel rates.

Figure 2 shows signatures of both fast and slow tunnel rates. The gray-scale reports g versus V_M for repeated sweeps of V_M through the same voltage range. For these sweeps, the dwell time per data point is 250 ms, and the voltage step per data point is 2 mV in Figs. 2(a) and 2(c) and 1 mV in Figs. 2(e) and 2(g). The horizontal axis is an index i representing the sweep number. Near the top of Fig. 2(a), the gray lines corresponding to charge transitions are straight and smooth: electrons hop out of the dot as soon as the dot chemical potential crosses the Fermi level of the leads, and the tunneling time τ is small compared with the dwell time per data point. As V_M is made more negative, the number of electrons in the dot decreases, and at the same time cross-talk between gate M and the quantum dot entrance and exit point contacts reduces the tunnel coupling between the dot and the leads, increasing τ . Eventually τ approaches and then exceeds the dwell time per data point, and near the bottom of panel (a) the horizontal lines are no longer smooth but rather exhibit random fluctuations. An important feature of the data in Fig. 2 is that the breaking up of the charge transition lines is gradual in Fig. 2(a), the line at $V_M = -0.48$ V is smooth and straight, and the next two lines, while clearly in the limit of slow τ , are nonetheless easily discernible. Figure 2(b) shows

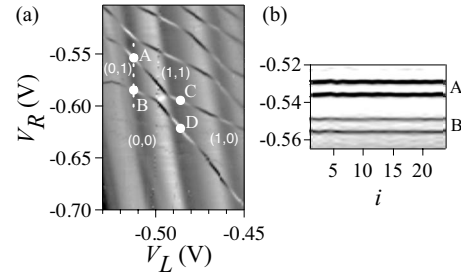


FIG. 3. One-electron Si/SiGe double quantum dot. (a) Charge stability diagram showing the QPC transconductance g . (b) Time-averaged pulsed-gate charge sensing with a 50 kHz square wave of peak-to-peak amplitude 7 mV added to V_R : g as a function of V_R along the white dashed line in (a).

a schematic representation of the potential landscape of the dot for the conditions of panel (a).

Figures 2(c) and 2(d) show plots analogous to Figs. 2(a) and 2(b), with the voltages V_L and V_R changed to increase the coupling to the left lead at the expense of that to the right lead. Because the tunnel couplings act in parallel, such a procedure reduces the tunneling time τ , and one expects to see smoother horizontal lines. In Fig. 2(c), the vertical axis is offset to correct for the effect of changing V_L and V_R , lining up the same charge transitions in Figs. 2(a) and 2(c). The second to last charge transition is now straight and smooth, while the last transition is still uneven. Note that the sensitivity of the charge-sensing point contact to electron tunneling events is also improved in Fig. 2(c) compared with Fig. 2(a) because the changes in gate voltage shift the position of the dot to the left, closer to the charge sensing channel. Figures 2(e) and 2(f) show the results of repeating this procedure; again, identical charge transitions are aligned. All of the lines are now straight and smooth, no additional lines have appeared below the final transition, and the sensitivity of the charge sensing is higher still.

The conditions in Fig. 2(e) correspond to tunnel rates fast enough that relatively high-frequency pulsed-gate voltage measurements³¹ can be performed. Figure 2(g) shows the time-average of the conductance g in the presence of a square wave of constant peak-to-peak amplitude 10 mV added to V_L . In Fig. 2(g), every transition line has split into two lines with no change in intensity as a function of frequency for frequencies up to 2 MHz, indicating that the loading and unloading rates of electrons into and out of the dot are faster than the pulse frequency over this entire frequency range.

We now reconfigure the voltages on the gates and move smoothly from the one-electron single dot regime to the one-electron double dot regime. To split the single dot into a double dot, V_T is made more negative, and the other gate voltages are adjusted to keep the one electron line visible. Figure 3(a) is a plot of g as a function of V_L and V_R in the double dot regime, showing the characteristic “honeycomb” charge transition lines. The extended empty region toward the lower left corner corresponds to the (0,0) charge configuration. We characterize the tunnel rates at points A and B by applying voltage pulses to gate R . Figure 3(b) shows g as a function of the sweep index i and V_R , with a 50 kHz square-wave pulse of peak-to-peak amplitude 7 mV added to V_R . The charge transition lines at A and B in Fig. 3(a), split into two smooth lines in Fig. 3(b), demonstrating that the tunnel rates are at least of the order of 50 kHz, and that the tunnel-

ing times τ are much faster than the dwell time per data pixel in Fig. 3(a), which is 200 ms. A measurement performed at the locations of points C and D in Fig. 3(a) yields similar results. Note that the data in Fig. 3(a) and that in Fig. 3(b) were taken on different days, explaining the small shift in the operating point between the two sets of data.

We have presented charge sensing data for single and double Si/SiGe quantum dots in the one-electron regime. We find that tuning the gate voltages provides good control over the tunnel rates in this regime, and that pulsed gate voltage measurements can be performed on both single and double dots. For the single dot, we have demonstrated tunnel rates in excess of 2 MHz, and for the one electron double dot, we observe tunnel rates in excess of 50 kHz to each of the leads. Further increases in tunnel rates are likely to be achievable by changing the size of the gate pattern.

This work was supported in part by ARO and LPS (Grant No. W911NF-08-1-0482), by NSF (Grant No. DMR-0805045), by United States Department of Defense, and by DOE (Grant No. DE-FG02-03ER46028). The views and conclusions contained in this document are those of the authors and should not be interpreted as representing the official policies, either expressly or implied, of the U.S. Government. This research utilized NSF-supported shared facilities at the University of Wisconsin-Madison.

- ¹D. Loss and D. P. Divincenzo, *Phys. Rev. A* **57**, 120 (1998).
- ²J. M. Elzerman, R. Hanson, L. H. W. van Beveren, B. Witkamp, L. M. K. Vandersypen, and L. P. Kouwenhoven, *Nature (London)* **430**, 431 (2004).
- ³J. R. Petta, A. C. Johnson, J. M. Taylor, E. A. Laird, A. Yacoby, M. D. Lukin, C. M. Marcus, M. P. Hanson, and A. C. Gossard, *Science* **309**, 2180 (2005).
- ⁴F. H. L. Koppens, C. Buizert, K. J. Tielrooij, I. T. Vink, K. C. Nowack, T. Meunier, L. P. Kouwenhoven, and L. M. K. Vandersypen, *Nature (London)* **442**, 766 (2006).
- ⁵C. Tahan, M. Friesen, and R. Joynt, *Phys. Rev. B* **66**, 035314 (2002).
- ⁶A. M. Tyryshkin, S. A. Lyon, A. V. Astashkin, and A. M. Raitsimring, *Phys. Rev. B* **68**, 193207 (2003).
- ⁷R. de Sousa and S. Das Sarma, *Phys. Rev. B* **68**, 115322 (2003).
- ⁸B. E. Kane, *Nature (London)* **393**, 133 (1998).
- ⁹R. Vrijen, E. Yablonovitch, K. Wang, H. W. Jiang, A. Balandin, V. Roychowdhury, T. Mor, and D. Divincenzo, *Phys. Rev. A* **62**, 012306 (2000).
- ¹⁰M. Friesen, P. Rugheimer, D. E. Savage, M. G. Lagally, D. W. van der Weide, R. Joynt, and M. A. Eriksson, *Phys. Rev. B* **67**, 121301 (2003).
- ¹¹L. C. L. Hollenberg, A. D. Greentree, A. G. Fowler, and C. J. Wellard, *Phys. Rev. B* **74**, 045311 (2006).
- ¹²A. Morello, C. C. Escott, H. Huebl, L. H. W. van Beveren, L. C. L. Hollenberg, D. N. Jamieson, A. S. Dzurak, and R. G. Clark, *Phys. Rev. B* **80**, 081307 (2009).
- ¹³K. A. Slinker, K. L. M. Lewis, C. C. Haselby, S. Goswami, L. J. Klein, J. O. Chu, S. N. Coppersmith, R. Joynt, R. H. Blick, M. Friesen, and M. A. Eriksson, *New J. Phys.* **7**, 246 (2005).
- ¹⁴T. Berer, D. Pachinger, G. Pillwein, M. Mühlberger, H. Lichtenberger, G. Brunthaler, and F. Schäffler, *Appl. Phys. Lett.* **88**, 162112 (2006).
- ¹⁵S. J. Angus, A. J. Ferguson, A. S. Dzurak, and R. G. Clark, *Nano Lett.* **7**, 2051 (2007).
- ¹⁶Y. Hu, H. O. H. Churchill, D. J. Reilly, J. Xiang, C. M. Lieber, and C. M. Marcus, *Nat. Nanotechnol.* **2**, 622 (2007).
- ¹⁷N. M. Zimmerman, B. J. Simmonds, A. Fujiwara, Y. Ono, Y. Takahashi, and H. Inokawa, *Appl. Phys. Lett.* **90**, 033507 (2007).
- ¹⁸N. Shaji, C. B. Simmons, M. Thalakulam, L. J. Klein, H. Qin, H. Luo, D. E. Savage, M. G. Lagally, A. J. Rimberg, R. Joynt, M. Friesen, R. H. Blick, S. N. Coppersmith, and M. A. Eriksson, *Nat. Phys.* **4**, 540 (2008).
- ¹⁹H. W. Liu, T. Fujisawa, Y. Ono, H. Inokawa, A. Fujiwara, K. Takashina, and Y. Hirayama, *Phys. Rev. B* **77**, 073310 (2008).
- ²⁰G. P. Lansbergen, R. Rahman, C. J. Wellard, I. Woo, J. Caro, N. Collaert, S. Biesemans, G. Klimeck, L. C. L. Hollenberg, and S. Rogge, *Nat. Phys.* **4**, 656 (2008).
- ²¹A. Fuhrer, M. Fuchsle, T. C. G. Reusch, B. Weber, and M. Y. Simmons, *Nano Lett.* **9**, 707 (2009).
- ²²C. B. Simmons, M. Thalakulam, B. M. Rosemeyer, B. J. V. Bael, E. K. Sackmann, D. E. Savage, M. G. Lagally, R. Joynt, M. Friesen, S. N. Coppersmith, and M. A. Eriksson, *Nano Lett.* **9**, 3234 (2009).
- ²³E. P. Nordberg, G. A. T. Eyck, H. L. Stalford, R. P. Muller, R. W. Young, K. Eng, L. A. Tracy, K. D. Childs, J. R. Wendt, R. K. Grubbs, J. Stevens, M. P. Lilly, M. A. Eriksson, and M. S. Carroll, *Phys. Rev. B* **80**, 115331 (2009).
- ²⁴R. R. Hayes, A. A. Kiselev, M. G. Borselli, S. S. Bui, E. T. Croke, III, P. W. Deelman, B. M. Maune, I. Milosavljevic, J.-S. Moon, R. S. Ross, A. E. Schmitz, M. F. Gyure, and A. T. Hunter, arXiv:0908.0173v1 (unpublished).
- ²⁵M. Xiao, M. G. House, and H. W. Jiang, *Phys. Rev. Lett.* **104**, 096801 (2010).
- ²⁶C. B. Simmons, M. Thalakulam, N. Shaji, L. J. Klein, H. Qin, R. H. Blick, D. E. Savage, M. G. Lagally, S. N. Coppersmith, and M. A. Eriksson, *Appl. Phys. Lett.* **91**, 213103 (2007).
- ²⁷W. H. Lim, F. A. Zwanenburg, H. Huebl, M. Möttönen, K. W. Chan, A. Morello, and A. S. Dzurak, *Appl. Phys. Lett.* **95**, 242102 (2009).
- ²⁸F. A. Zwanenburg, C. E. W. M. V. Rijmenam, Y. Fang, C. M. Lieber, and L. P. Kouwenhoven, *Nano Lett.* **9**, 1071 (2009).
- ²⁹J. Taylor, H. Engel, W. Dur, A. Yacoby, C. Marcus, P. Zoller, and M. Lukin, *Nat. Phys.* **1**, 177 (2005).
- ³⁰M. Ciorga, A. S. Sachrajda, P. Hawrylak, C. Gould, P. Zawadzki, S. Julian, Y. Feng, and Z. Wasilewski, *Phys. Rev. B* **61**, R16315 (2000).
- ³¹J. Elzerman, R. Hanson, L. van Beveren, L. Vandersypen, and L. Kouwenhoven, *Appl. Phys. Lett.* **84**, 4617 (2004).